Macromolecules
A R T I C L E

Gyroid-Forming Diblock Copolymers Confined in Cylindrical Geometry: A Case of Extreme Makeover for Domain Morphology

Minglin Ma,[*,†,§] **Edwin L. Thomas,**[‡,§] **and Gregory C. Rutledge**[†,§]

[†]*Department of Chemical Engineering,* [‡]*Department of Material Science and Engineering, and* [§]*Institute for Soldier Nanotechnologies, Massachusetts Institute of Technology, Cambridge, Massachusetts 02139*

Bin Yu, Baohui Li,* Qinghua Jin, and Datong Ding

School of Physics, Nankai University, Tianjin 300071, P. R. China

An-Chang Shi

Department of Physics and Astronomy, McMaster University, Hamilton, Ontario L8S 4M1, Canada

Received October 11, 2009; Revised Manuscript Received February 11, 2010

ABSTRACT: The self-assembly of gyroid-forming diblock copolymers confined in cylindrical geometry is studied using a combination of computer simulations and experiments. The simulations, based on a system qualitatively representative of poly(styrene-*b*-isoprene), are performed with cylindrical nanopores of different diameter (D) and surface selectivity. The effects of the pore size and surface selectivity on morphology are systematically investigated. Different morphological sequences are predicted for two gyroid-forming diblock copolymers. The experiments are carried out on two gyroid-forming poly(styrene-*b*-dimethylsiloxane) block copolymer samples confined in the core of continuous core−shell nanofibers of different diameters, which are obtained by a coaxial two-fluid electrospinning technique. The internal microphase-separated morphologies of these fibers are investigated by transmission electron microscopy (TEM). Both simulations and experiments demonstrate that a rich variety of structures spontaneously form for the gyroid-forming diblock copolymers, depending on the conditions of cylindrical confinement. Many of these confinement-induced structures are quite different from those of cylinder-forming or lamella-forming block copolymers. Simulations further show that these structures depend sensitively on the block copolymer composition, surface selectivity, and the ratio D/L_0 where L_0 is the period of the equilibrium gyroid phase. While the simulation and experimental systems are representative of different chemistries, the morphological predictions of simulations are qualitatively consistent with the experimental observations.

Introduction

In many technological and biological applications, materials that spontaneously form ordered bulk phases may be confined in a small space, leading to the formation of complex morphologies not observed in the bulk. One such example is a block copolymer confined in a cylindrical pore with diameter of a few (typically < 10) times the fundamental period of the bulk morphology. Diblock copolymers (DBCPs), the simplest case of block copolymers, are linear polymers composed of two different subchains (A and B blocks). Their phase behavior in bulk is controlled by the competition between the A−B repulsion and chain connectivity. The bulk phase diagram of DBCPs has been well studied in both theories and experiments.[1,2] A number of ordered equilibrium phases, including lamellae, hexagonally packed cylinders, body-centered-cubic spheres, cubic double gyroid (DG) phase (a bicontinuous networked structure),[3] and perforated lamella (PL) structure,[4,5] can be formed. Very recently, an orthorhombic *Fddd* (O^{70}) networked structure was predicted to be stable in DBCP melts in a very narrow weak segregation region.[6]

Various novel and sometimes complex structures have been observed or predicted for block copolymers confined in cylindrical pores. Experimentally, Russell and co-workers carried out a series of studies on symmetric (bulk lamella-forming)[7−10] and asymmetric (bulk cylinder- and sphere-forming)[8−11] poly-(styrene-*b*-butadiene) (PS-*b*-PB) DBCPs confined in cylindrical nanopores in alumina membranes. For the lamella-forming symmetric PS-*b*-PB, a set of curved, cylindrical lamellae parallel to the pore axis (called "concentric lamellae", CL) were observed when the pore diameter D is much larger than the bulk equilibrium period L_0. Moreover, a novel stacked disk or toroid morphology is observed when D is comparable to L_0 and D/L_0 is not an integer.[7,10] For the cylinder-forming asymmetric PS-*b*-PB, cylinders oriented parallel to the pore axis are obtained within large pores ($D/L_0 > 4.1$). When the pore diameter is reduced to a size comparable to the bulk period ($D/L_0 = 0.92−2.2$), a rich variety of morphologies, not seen in the bulk, were observed that included stacked torus-like morphologies and single-, double-, and triple-helical morphologies.[10,11] Similarly, for the sphere-forming PS-*b*-PB, one observes that large pores ($D/L_0 > 3.2$) lead to spherical PB domains aligned along the pore axis, whereas in pores with smaller diameters ($D/L_0 < 3.2$), core−shell cylindrical morphologies, single columns of spherical microdomains, and spirals of doubly and triply paired spherical microdomains are observed.[9,10] Helical and stacked toroidal structures have also been observed by Wang and co-workers in the study of asymmetric poly(styrene-*b*-2-vinylpyridine)

*To whom correspondence should be addressed: e-mail minglin@mit.edu, tel (617) 324-9163 (M.M.); e-mail baohui@nankai.edu.cn (B.L.).

DBCPs confined in anodic aluminum oxide nanopores.[12] Concentric lamellar (CL) structures have been observed by Sun and co-workers in the study of symmetric poly(styrene-*b*-methyl methacrylate) DBCPs confined in alumina nanopores.[13] Similarly, Kalra et al.[14] and Ma et al.[15] observed the formation of the CL morphology in electrospun block copolymer nanofibers. Ma and co-workers also observed spheres arranged in concentric cylindrical shells in sphere-forming copolymers.[15]

Complementary to these experimental investigations, the cylindrically confined DBCPs have also been extensively studied using theory and simulations. He et al.[16] and Sevink et al.[17] studied the self-assembled morphologies of symmetric DBCPs confined in cylindrical pores using Monte Carlo and dynamical density functional simulations, respectively. They observed concentric lamellae for cylindrical pores with an inner surface that strongly prefers one component of the DBCP over the other[16] and lamellae perpendicular to the pore axis (perpendicular lamellae or stacked disks) for cylindrical pores with neutral surfaces.[17] Recently, Li et al. performed real-space self-consistent-field theoretic (SCFT) calculations in two dimensions and constructed a phase diagram for DBCP melts confined in a circular geometry.[18] The SCFT results of Li et al. lead to the prediction of a number of interesting structures, including non-hexagonally packed cylinders and structures that are intermediate between lamellae and cylinders. These studies provide an understanding of the DBCP phase behavior under cylindrical confinement.[18] However, some of the structures observed in experiments, such as perpendicular lamellae, helices, and stacked toroids, are not invariant in the third dimension (i.e., along the pore axis) and cannot be obtained by calculations in only two dimensions. Therefore, it is necessary to explore the phase diagram in three-dimensional space. In the past few years, many novel structures, such as porous lamella (mesh) structures, lamellae parallel to the pore axis (parallel lamellae), and helices, were predicted using computer simulations for lamella-forming DBCPs confined in nanopores.[19-25] For cylinder-forming DBCPs, it has been shown by simulations[23-26] and SCFT calculations[27,28] that novel structures such as helices and stacked toroids spontaneously form inside the cylindrical pore. On the other hand, various concentric perforated lamellae-related structures were also predicted by simulations[25] and SCFT calculations[28] for cylinder-forming DBCPs having compositions located near the cylinder−gyroid phase boundary. It can be concluded that confinement within a cylindrical geometry can lead to the formation of very rich diversity of structures.

The formation of complex structures due to confinement can be understood in general by considering a few key factors, the most important being symmetry matching between the confining geometry and the preferred bulk morphology of the block copolymer and surface interaction between the confining material and the block copolymer components.[29] For example, in the case of lamellae-forming DBCP confined in a cylindrical pore, the confinement is two-dimensional and possesses a uniaxial symmetry, while the lamellar bulk phase is periodic in one dimension. When the confining surface is neutral, an obvious solution for the confinement of lamellae in a cylindrical pore is to align the dimension of periodicity of the lamellar morphology along the axis of the cylinder, so that the point group symmetry of the lamellae in this orientation is consistent with the point group of the cylinder. However, when the confining surface has a strong preference for one of the blocks, the copolymer may be forced to accommodate to the geometry of the confining space, leading to frustrations of the bulk structure and thus the formation of defects. In many cases defects such as dislocations and disclinations are introduced to minimize the frustration of the preferred bulk packing. One example is found in a myelin figure, which is a lamellar phase curved into a concentric set of shells with a +1 disclination defect at the central axis. In this case the concentric arrangement of the lamellae represents the best way to release the packing frustration. To accommodate variations in confinement diameter, Ma et al. have reported observation of a radial edge dislocation loop, which occurs when the number of layers in a myelin figure increase or decrease by 1/2.[30]

Placing gyroid-forming block copolymers in cylindrical geometry becomes a significantly more complicated problem because of the unavoidable mismatch between the cubic symmetry of the bulk morphology, with continuity in both domains, and the uniaxial symmetry of the confinement geometry. The basic shape of the gyroid is a 3-fold junction of three arms, in which each arm connects to another set of three arms that are each themselves rotated by 71° with respect to the plane of the first set of arms, resulting in a 3D network that has helical twist along $\langle 111 \rangle$ and $\langle 100 \rangle$ directions.[31] Moreover in the double gyroid morphology (DG), there exists a second 3D domain network that is twisting in the opposite sense along the $\langle 111 \rangle$ and $\langle 100 \rangle$ directions. This bicontinuous structure has many potential technological applications such as precursors for nanoporous materials.[32,33] Confining a gyroid-forming block copolymer inside a cylinder is likely to be very costly in terms of free energy, promoting the transformation to a nearby morphology, such as lamellae or cylinders, or even to an entirely new packing scheme whereby the gyroid network can accommodate its complex set of interface shapes and dimensions between domains inside the cylinder. One possibility to resolve the symmetry mismatch is to look for a continuous path in the DG structure and direct it along the axis of the cylinder, while at the same time the bicontinuous network must terminate in the directions normal to the cylinder axis, maintaining overall composition, curvature, and distances between block interfaces. This represents a difficult geometry problem and an example of extreme makeover of morphologies. In order to gain insight into the understanding of this challenging problem, experimental and simulation studies of gyroid-forming block copolymers confined in cylindrical geometries, either nanopores or nanofibers, are carried out, and the results are reported in this paper.

Simulation Details

The simulations are based on a simulated annealing method[34] applied to a "single-site bond fluctuation" model of polymers.[35,36] Simulated annealing method is a well-known procedure for obtaining the lowest energy "ground states" in disordered systems.[37,38] To use the method, four factors need to be specified: an initial configuration, a set of trial moves with sufficient power to enable all relevant states to be generated, an energy function, and a schedule for decreasing the temperature. In the present study, these factors are specified in the following paragraphs. Starting from the specified initial configuration, the simulations are carried out by executing a series of Monte Carlo simulations with each at a different temperature and called a step. The temperature in the initial step is high enough to allow most of the trial moves to be accepted, and it is decreasing with the specified schedule in the following steps. The final configuration for a given step is subsequently taken as the starting point for the next step at a slightly lower temperature. At each step, enough trial moves are performed to allow the system to reach equilibrium at the corresponding temperature. Finally, the ground state of the system is obtained.

Bulk simulations are performed first for the model DBCPs to locate the gyroid phase in the composition space. The morphologies formed under confinement in cylindrical nanopores are then obtained. The model DBCP chains used in the simulations are of the type A_n-b-B_{N-n}, where N is the number of monomers and n is the number of A-monomers. It has been established in previous studies that for the DBCPs A_n-b-B_{N-n} with N = 12

gyroids are formed at $n = 4$, whereas lamellae and hexagonally packed cylinders are formed at $n = 6$, 5 and 3, 2, respectively.[26] Thus, for the neat DBCPs A_n-b-B_{12-n} with a single n, gyroid phase can be obtained only when the fraction of A-monomers $f_A = 1/3$ due to the narrow f_A window of the gyroid phase in the phase diagram. In order to probe the parameter (f_A) region in which the gyroid is stable with greater resolution, and also to get more gyroid-forming systems with different f_A values, we employ a blend system that contains two types of DBCPs, A_n-b-B_{12-n} and A_{n+1}-b-B_{12-n-1}, where n is an integer. The blend is used just for adjusting the f_A value, so that f_A can change continuously in our model. In each blend, the ratios of the two types of DBCP chains out of the total chains are denoted as p_1 and $(1 - p_1)$, respectively. The effective volume fraction of A-blocks in the blend is $f_A = [np_1 + (n+1)(1 - p_1)]/12$. To check the influence of f_A on the final phase behavior of confined gyroid-forming block copolymers, gyroid-forming DBCP systems with a single type of DBCP chains ($f_A = 1/3$) and a blend of two types of DBCP chains are used in our study.

For all the simulations, the model system is embedded in a simple cubic lattice of volume $V = L_X \times L_Y \times L_Z$. Each monomer occupies one lattice site, and the polymers are self-avoiding and mutually avoiding. The bond length can assume values of 1 or $\sqrt{2}$, in lattice units, so that each site has up to 18 nearest-neighbor sites. The total monomer concentration in the system is kept at a constant $\rho = 85\%$. For the simulation of the bulk phases, periodic boundary conditions are applied in all three directions. For the gyroid phase, we use $L_X = L_Y = L_Z = L$ unless otherwise specified, due to the cubic symmetry of the structure. For the simulation of confined self-assembly, gyroid-forming DBCPs are confined to a long cylindrical pore of diameter D. The pore axis is along the z direction and the periodic boundary condition is applied to the z direction. The pore consists of those lattice sites whose distance to the pore axis is equal to or smaller than $D/2$. The lattice sites outside the pore constitute the pore wall. Polymers cannot occupy the wall sites. In all cases, only nearest-neighbors interactions are considered. The repulsive interaction between the A monomers and B monomers is modeled by a parameter $\varepsilon_{AB} = 1.0k_BT_{ref}$, where k_B is the Boltzmann constant and T_{ref} is a reference temperature. The A−A and B−B interactions are set to be $\varepsilon_{AA} = \varepsilon_{BB} = 0$. The interactions between the pore wall and monomers are set to be $\varepsilon_{WA} = \alpha\varepsilon_{AB}$ and $\varepsilon_{WB} = -\alpha\varepsilon_{AB}$. Depending on the interactions between the wall and polymers, three types of pores are considered: (1) the pore is neutral ($\alpha = 0$), (2) the pore is strongly attractive to the majority block ($\alpha = 1$), and (3) the pore is strongly attractive to the minority block ($\alpha = -1$).

The initial configuration is generated by putting a maximum number of copolymer chains onto the lattice first. The polymer chains are parallel to one of the lattice axes and are either in an extended or once-folded conformation. Randomly chosen chains are then removed from the box until the desired volume fraction (0.85) is reached. Two types of trial moves, chain reversal and exchange moves, are used in the simulations, which are the same as those used in our previous studies.[39−41] The acceptance or rejection of the attempted move is governed by whether it breaks the chain and further by the Metropolis rule.[42] Starting from this initial state at $T = 30T_{ref}$, the ground state of the system is obtained by a simulated annealing protocol with decreasing T by a factor of 0.92 or 0.95 with each successive simulation until 70 annealing steps are reached. At each annealing step, 25 000 Monte Carlo steps are performed. One Monte Carlo step is defined as the number of moves required, on average, for all the chains to be reversed and all the lattice sites to be visited one time.

For the neat and blend DBCP systems with chain length $N = 12$, a phase diagram has been constructed in the composition
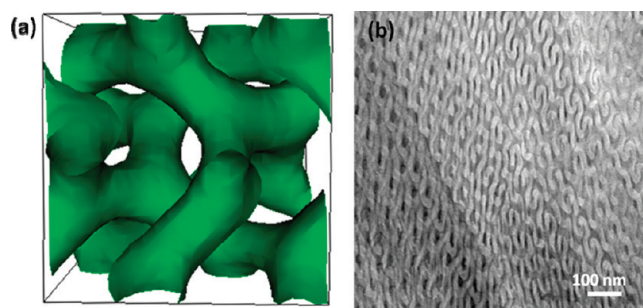
Figure 1. (a) Snapshot of gyroid phase formed for system with $f_A = 0.3$ in a cubic box with $L_0 = 24$; only the A-domains are shown. The distances between two closest parallel rods and perpendicular rods are $(5/16)^{1/2}L_0$ (or 13.4) and $1/2L_0$ (or 12), respectively. (b) TEM image of the gyroid-forming PS-b-PDMS-75 DBCP in bulk. The dark domains are PDMS, and the light ones are PS.

range $1/6 \leq f_A \leq 1/2$. Gyroids are formed in the neat DBCP A_4-b-B_8 and in the blends of A_4-b-B_8 with A_3-b-B_9 (blend 1) or A_5-b-B_7 (blend 2) when the ratio of A_4-b-B_8 in the blends is in the range of $p_1 \geq 0.4$ or $p_1 \geq 0.6$, respectively. Hexagonally packed cylinders are formed in the range of $p_1 < 0.4$ for blend 1, and lamellae are formed in the range of $p_1 < 0.6$ for blend 2. This result corresponds to that the range of volume fraction for which gyroid structure occurs in our simulation is $0.283 \leq f_A \leq 0.366$. On the other hand, it is also noticed that near the boundaries between different phases there exist degenerated structures of cylinders and gyroids for blend 1 when $0.40 \leq p_1 \leq 0.45$ and of lamellae or perforated lamellae and gyroids for blend 2 when $0.60 \leq p_1 \leq 0.70$. Therefore, the range of volume fraction for which stable gyroid structure occurs in our simulation is $0.29 \leq f_A \leq 0.35$. Our further simulations for neat diblock copolymers with longer chains accord with this result. A recent SCFT calculation shows that the stable window for gyroid formation is $0.338 < f_A < 0.375$ in the weak segregation regime ($\chi N = 20$) and shifts to $0.306 < f_A < 0.321$ in the strong segregation regime ($\chi N = 100$).[43] The range of volume fraction for which stable gyroid structure occurs in our simulation is slightly wider than that predicted by SCFT,[43] possibly due to differences in the models used. Because the two types of DBCPs, A_n-b-B_{12-n} and A_{n+1}-b-B_{12-n-1}, are very similar to each other, it is expected that the resulting phase diagram can be used to represent the phase diagram of neat DBCPs according to SCFT theory calculations.[44] For the confined system, gyroid-forming DBCP systems with the neat A_4-b-B_8 chains ($f_A = 1/3$) and blends of two types of chains, A_4-b-B_8 and A_3-b-B_9 ($p_1 = 0.6$ or $f_A = 0.3$), are employed. The system with $f_A = 0.3$ is close to the cylinder−gyroid phase boundary whereas that with $f_A = 1/3$ is close to the gyroid−lamella phase boundary.

In previous studies, it has been shown that having a good estimate of the bulk period L_0 for confined simulations is crucial.[21,45] This is especially true for the gyroid structure because it can only occur for certain specific box sizes in our simulations. Therefore, simulations on bulk systems with various box sizes were performed first to obtain the characteristic period L_0 for the gyroid structures. In a previous study, we have reported that for the model DBCP system A_4-b-B_8 the bulk period of the gyroid phase is $L_0 = 24$ (in lattice units).[46] For the blend system with $f_A = 0.3$, our simulations predict that the bulk period of the gyroid phase is also $L_0 = 24$. The final morphology of the gyroid phase formed by the DBCPs at $f_A = 0.3$ with one period is shown in Figure 1a. To verify the reliability of the resulting L_0 value, we performed simulations in a rectangular box with lengths of $L_X = L_Y = 24$ and $L_Z = 48$. We found that such a box can produce gyroid structure with two periods in the Z direction and one period in the other two directions. Therefore, we are confident

that our results about the bulk period are not affected by the finite computational boxes. Furthermore, we have checked the simulated structures by calculating the structure factor based on the method proposed previously.[47] The calculated spherically averaged structure factor of the simulated structure is in good agreement with the experimental SAXS spectra of the gyroid structure.[48] Therefore, one can incontestably identify the simulated structure as that of the gyroid.

Experimental Details

Electrospinning is a facile technique for forming continuous nanofibers, with diameters typically between 10 nm and 10 μm, from polymer solutions or melts.[49] In our experimental studies, we use the recently developed coaxial two-fluid electrospinning technique[50−52] to direct the self-assembly of block copolymers under cylindrical confinement within nanofibers. In our variation of the method,[15] a solution of the block copolymer is processed as the core component and a solution of a second polymer with high glass transition temperature (T_g) is used as the shell material. The two fluids are then electrospun coaxially using two concentric

Table 1. Operating Parameters for the Two-Fluid Electrospinning of the Two Different DBCPs

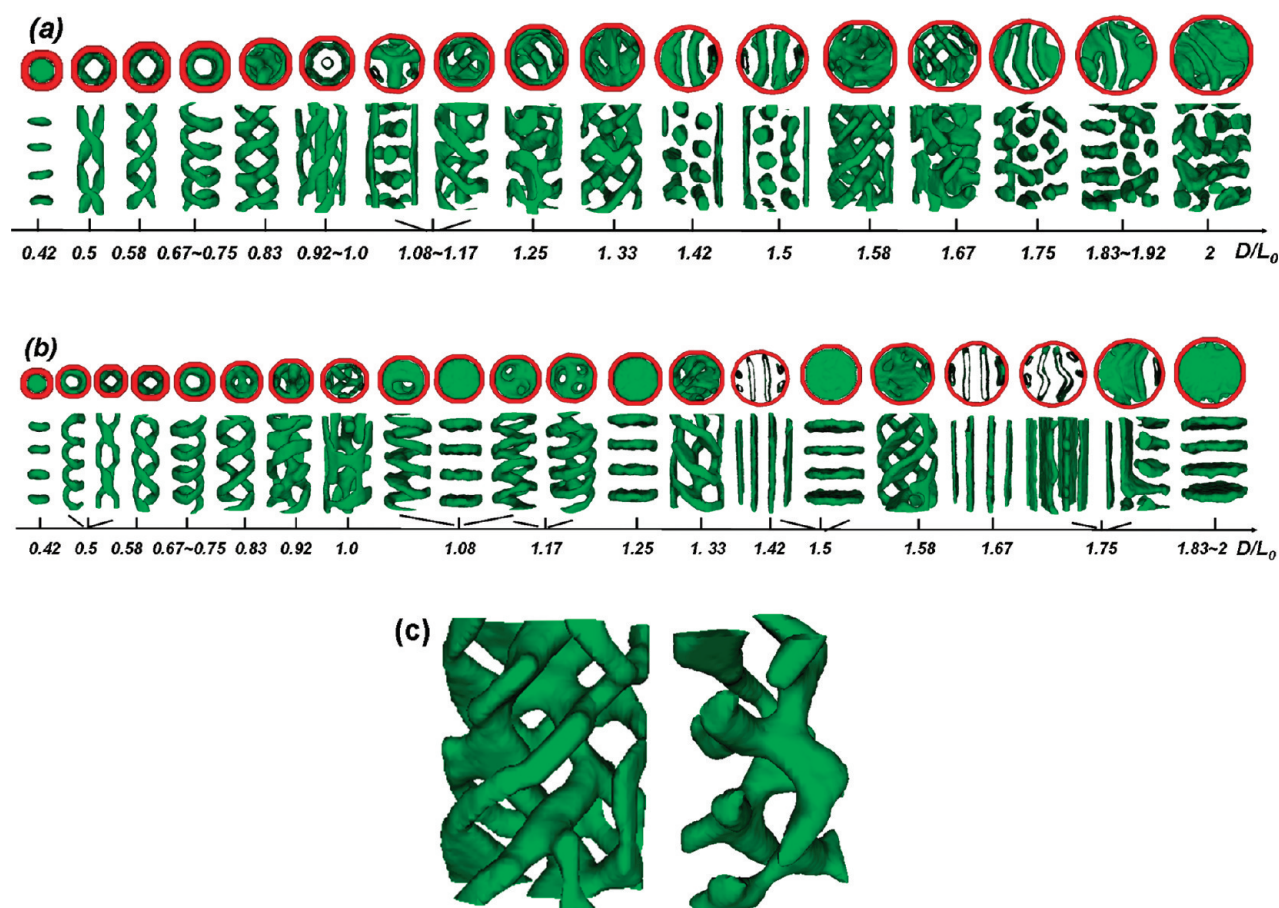| DBCP	voltage (kV)	plate-to-plate distance (cm)	shell flow rate (mL/min)	core flow rate (mL/min)
PS-b-PDMS-75	35	45	0.04	0.005
PS-b-PDMS-136	38	45	0.06	0.003

spinnerets. Upon evaporation of the solvents, a continuous filament is obtained with the block copolymer in the core and the thermally stable polymer in the shell. Subsequent annealing of the fiber at a temperature higher than the uppermost T_g of the block copolymer but lower than that of the shell material leads to self-assembly of the block copolymer under cylindrical confinement.

The samples used were poly(styrene-b-dimethylsiloxane) (PS-b-PDMS) DBCPs.[53] The first PS-b-PDMS DBCP (PS-b-PDMS-75) has a total molecular weight (M_w) of 75.5 kDa, polydispersity index (PDI) of 1.04, and PDMS volume fraction $f_{PDMS} = 0.415$. It forms the double-gyroid structure in bulk with [211] spacing (d_{211}) of 61 nm, as determined by small-angle X-ray scattering (SAXS). Figure 1b shows a transmission electron microscopy (TEM) image of the bulk sample. The second gyroid-forming PS-b-PDMS DBCP (PS-b-PDMS-136; M_w = 136.1 kDa; $f_{PDMS} = 0.411$; PDI = 1.09; d_{211} = 80 nm) has PDI and PDMS volume fraction similar to the first sample but a higher molecular weight and bulk period. A poly(methacrylic acid) (PMAA) polymer (Scientific Polymer Products, Inc.) was used as the shell material. It has a T_g of 220 °C, much higher than that of either PS (105 °C) or PDMS (−120 °C).[54]

The fibers were made using a two-fluid coaxial electrospinning technique with 22 wt % PMAA in dimethylformamide (DMF; Sigma-Aldrich Co.) as the shell fluid and 13 wt % PS-b-PDMS-75 (or 7 wt % PS-b-PDMS-136) in a solvent mixture of chloroform (Sigma-Aldrich Co.) and DMF (CHCl$_3$/DMF = 3:1 by volume) as the core fluid. The operating parameters are shown in Table 1. The resulting core/shell fibers were then annealed at 160 °C (for PS-b-PDMS-75) or 170 °C (for PS-b-PDMS-136) for 10 days

Figure 2. Self-assembled morphologies for gyroid-forming DBCPs as a function of D/L_0 confined in neutral pores ($\alpha = 0$) for a system with (a) $f_A = 0.3$ and (b) $f_A = 1/3$, respectively. Both a top view and a side view of A-domains are given. The outermost circle in each top view indicates the surface of the cylindrical pore. (c) The continuous networked structure formed at $D/L_0 = 1.58$ for system with $f_A = 0.3$; the inner part is shown separately and is truncated within a pore diameter $D/L_0 < 1.33$.
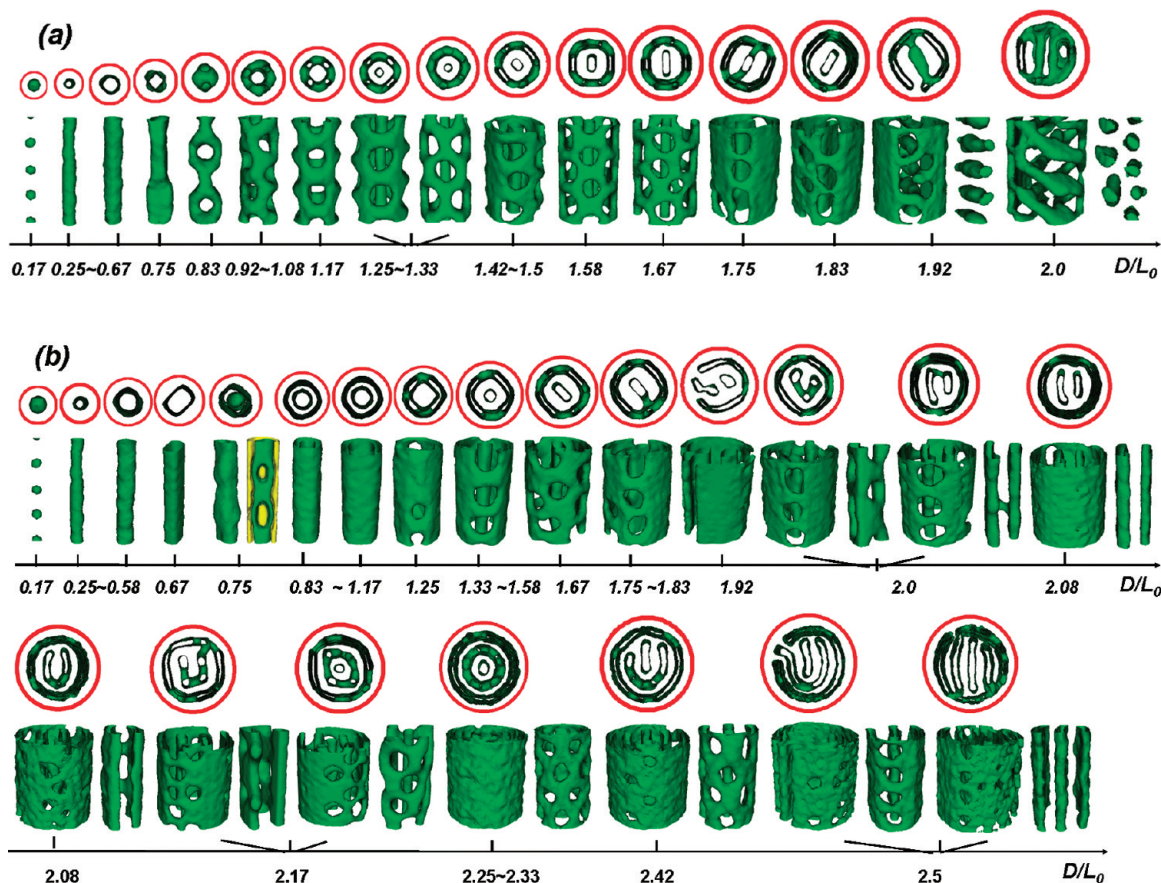
Figure 3. Self-assembled morphologies for gyroid-forming DBCPs as a function of D/L_0 confined in majority-selective pores ($\alpha = 1$) for system with (a) $f_A = 0.3$ and (b) $f_A = 1/3$, respectively. Both a top view and a side view of A-domains are given. The outermost circle in each top view indicates the surface of the cylindrical pore. For some large pores, the inner structure or a cross-section structure is shown separately. In each side view in Figure 3b, with $D/L_0 > 2.0$ the size along the pore axis direction is doubled by periodic replication of the simulated size.

under vacuum (VWR Signature microprocessor-controlled vacuum oven). Because of the presence of the high-T_g PMAA, the fiber appearance and dimensions remained unchanged upon annealing, as observed by scanning electron microscopy (SEM).

The size and uniformity of the fibers were observed using SEM (JEOL-6060SEM from JEOL Ltd., Japan) after the fibers were sputter-coated with a 2−3 nm layer of gold (Desk II cold sputter/etch unit from Denton Vacuum LLC, NJ). Their internal morphologies were examined using TEM (JEOL JEM200 CX from JEOL Ltd., Japan). The TEM samples were prepared as follows. The annealed fibers were first embedded in epoxy resin (LR White-Medium grade, Ladd Research) and cryo-microtomed into ∼70 nm thick sections using a diamond knife (Diatome AG) on a microtome device (Leica EM UC6). The cutting temperature was set at −160 °C, lower than the T_g of both PS (105 °C) and PDMS (−120 °C),[54] to minimize distortions of microdomains during the microtoming. The cross sections were then transferred to TEM grids for examination. Since the electron density of the PDMS block is sufficiently high to provide the necessary contrast over the PS block, no staining was needed.

Results and Discussion

A. Predicted Morphologies of the Confined Systems. The simulations of the confinement-induced structures were carried out using DBCPs with $f_A = 0.3$ or $f_A = 1/3$, different pore diameters, and pore−polymer interactions. In this section, results are presented for three typical cases, in which the pore wall is neutral (case 1), strongly attractive to the majority blocks (case 2), and strongly attractive to the minority block (case 3). Morphological sequences for

different pore−polymer interactions are summarized in Figures 2−4. In each figure, two sequences are shown, corresponding to the systems with $f_A = 0.3$ and $f_A = 1/3$. In each sequence the morphologies are organized as a function of the ratio D/L_0, and each snapshot is viewed both parallel and perpendicular to the pore axis. In the case of small pores, the pore length L_Z was varied to examine its influence on the equilibrium morphologies. The simulation results show that the morphologies exhibit a weak dependence on the pore length L_Z used in the simulation; that is, when L_Z/L_0 is close to an integer, with $L_Z/L_0 = 1.0$ or 2.0, the final morphology is independent of L_Z, whereas when L_Z/L_0 deviates from an integer, there is a displacement of the morphologies on the D/L_0 axes. This conclusion is consistent with that obtained for the cylinder-forming system.[40] Therefore, the pore length (L_Z) is fixed as 48 lattice units (i.e., $L_Z/L_0 = 2.0$) for all simulations, except those in case 2 with $D/L_0 > 2.0$, where L_Z is fixed at 24 lattice units (i.e., $L_Z/L_0 = 1.0$). Several different random number generator seeds have been used to test the versatility of the observed structures. Good reproducibility of the morphologies was obtained.

Case 1: Neutral Pores ($\alpha = 0$). In this case, the pore−polymer interactions are the same for the A and B blocks, leading to a nonselective pore wall. Typical morphologies obtained for DBCPs with $f_A = 0.3$ and $f_A = 1/3$ are shown in parts (a) and (b) of Figure 2, respectively. Each composition is discussed here in turn. As shown in Figure 2a, for the composition $f_A = 0.3$, stacked disks perpendicular to the pore axis are observed when the pore is very small ($D/L_0 < 0.5$). The distance between two neighboring disks is $L_0/2$.
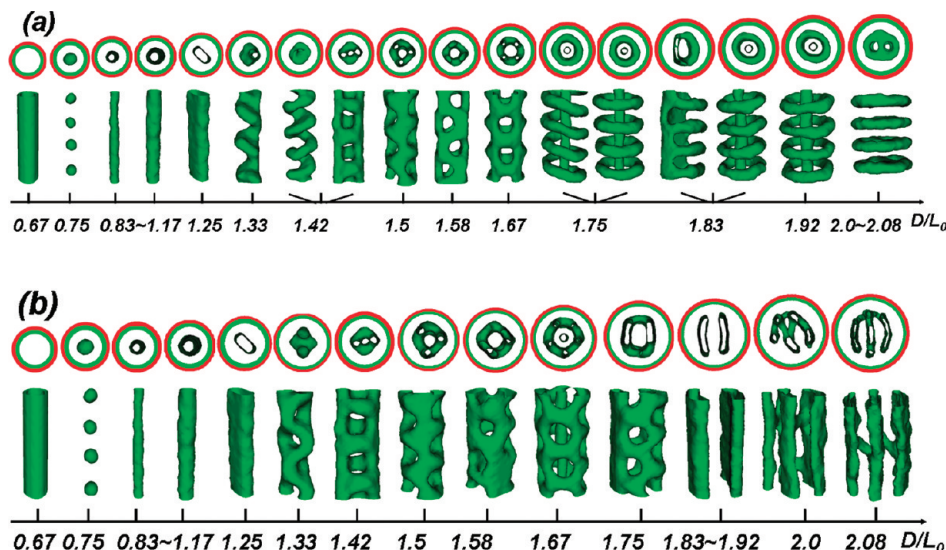
Figure 4. Self-assembled morphologies for gyroid-forming DBCPs as a function of D/L_0 confined in minority block selective pores ($\alpha = -1$) for system with (a) $f_A = 0.3$ and (b) $f_A = 1/3$, respectively. Both a top view and a side view of A-domains are given. The outermost circle in each top view indicates the surface of the cylindrical pore. The second circle from the outermost in each top view indicates the outermost A-layer, which is not shown in the side views for large pores.

With the increase of D/L_0, the stacked disks evolve into helical structures. Double helices (D-helix) and single helices (S-helix) are observed at $D/L_0 = 0.5-0.58$ and $D/L_0 = 0.67-0.75$, respectively. When D/L_0 is increased to 0.83, D-helices reoccur. However, the D-helices formed at $D/L_0 = 0.83$ consist of trifurcated cylinders which are different from those observed in smaller pores. It is interesting to notice that the pitch of the D-helices decreases with the increase of D/L_0 while the pitch of the S-helix is constant at $L_0/2$, independent of D/L_0. When $D/L_0 = 0.92-1.0$, structures with one cylinder at the center of the pore and five flattened cylinders that coil around the pore surface (denoted as C_1H_5) are observed. This is similar to the case of cylinder-forming DBCPs, where structures such as C_1H_4, C_1H_3, and C_1H_5, with one cylinder at the pore center and four, three, or five cylinders at the pore surface, were observed at $D/L_0 \approx 2.0$.[26,28,40] With a further increasing of D/L_0, helical structures disappear and more complex structures are observed in the pore. For pores with $D/L_0 = 1.08-2.0$, the typical morphologies can be classified into two categories. One category consists of continuous networked structures (with $D/L_0 = 1.08-1.33$, $1.58-1.67$), and the other consists of stacked cylinders perpendicular to the pore axis (perpendicular cylinders) (with $D/L_0 = 1.08-1.17$, $1.42-1.5$, and $1.75-2.0$). The continuous networked structures have not been observed before for the cylinder-forming or lamella-forming DBCPs under cylindrical confinement. These structures consist of branched cylinders in the inner pore connected with branched flat cylinders at the pore surface. The branched cylinders in the inner pore usually have triple junctions. It is interesting to notice that for the large pore at $D/L_0 \approx 1.6$ the continuous networked structure is very similar to the bicontinuous structure of bulk gyroid phase, as shown in Figure 2c. Thus, these continuous networked structures can be considered as the cylindrically confined counterpart of the bulk gyroid phase. On the other hand, when $D/L_0 = 1.08-1.17$, structure with one column of stacked trifurcated perpendicular cylinders is formed, acting as degenerated structures of the continuous networked structures. When $D/L_0 = 1.42$ or 1.5, structures with two columns of stacked perpendicular cylinders and one or two curved lamellae at the pore surface parallel to the pore axis

are formed. For the large pore at $D/L_0 = 1.75$, a structure with three columns of perpendicular cylinders is observed. With increasing the diameter of pore to $D/L_0 = 1.83-1.92$, the cylinders between different columns are connected so that a hybrid structure which is intermediate between stacked perpendicular cylinders and stacked perpendicular lamellae is observed. Finally, at $D/L_0 = 2.0$ the hybrid structure evolves into a stacked undulated lamella structure. The morphologies of stacked perpendicular cylinders resemble those observed in cylinder-forming DBCPs located near the cylinder-gyroid phase boundary confined in neutral cylindrical pores when D/L_0 is close to half-integers.[26] Chen et al. also observed deformed cylinders that bent into stacked toroids perpendicular to the pore axis when the pore diameter is incommensurate with the bulk period in cylinder-forming DBCPs whose composition is located near the cylinder-gyroid phase boundary.[28] As the gyroid-forming DBCP system ($f_A = 0.3$) is located close to the cylinder-gyroid phase boundary, morphologies similar to those observed in the cylinder-forming systems located near the cylinder-gyroid phase boundary are obtained.

As shown in Figure 2b for the system with $f_A = 1/3$, a morphological sequence similar to that obtained for the system with $f_A = 0.3$ is observed when the pore is small ($D/L_0 \leq 0.83$). The only difference is that the S-helix appears as a degenerated structure with the D-helix at $D/L_0 = 0.5$. The similarity in morphology between the two systems is reasonable since both of these DBCPs form gyroids in the bulk. However, the morphological sequence for the two systems differ for large pores ($D/L_0 > 1$). The continuous networked structures are observed for $f_A = 1/3$ at $D/L_0 = 0.92-1.0$, with higher degree of confinement than is the case for $f_A = 0.3$. When $D/L_0 = 1.08$, a set of degenerated structures including S-helix, connected stacked toroids, and perpendicular lamellae are observed. The pitch of the helix and the period of the connected stacked toroids or of the perpendicular lamellae have the same values of $L_0/2$. The connected stacked toroids are stable, and the S-helix evolves into a trifurcate S-helix at $D/L_0 = 1.17$. The structure of connected stacked toroids consists of stacked toroids and short cylinders, and the latter connect neighboring toroids. Similarly, the trifurcate S-helix consists of S-helix and

trifurcate cylinders, and the latter connect the former at some positions. When $D/L_0 = 1.25$, only perpendicular lamellae are observed, and they evolve into helical-lamellae at $D/L_0 = 1.33$. The helical lamella structure is a labyrinthine-like networked structure, similar to the continuous networked structure observed when $f_A = 0.3$. The main difference between them is that the latter is made up of connected cylinders, whereas the former is made up of connected lamellae. For the large pore at $D/L_0 = 1.42$, the helical lamellae transform into parallel lamellae. When $D/L_0 = 1.5$, two degenerated structures, including parallel lamellae and perpendicular lamellae, are observed. With further increase in the diameter of the pore in the range $D/L_0 = 1.5-1.67$, a transition sequence (perpendicular lamellae−helical lamellae−parallel lamellae), resembling that observed in the range of $D/L_0 = 1.25-1.42$, is observed. When $D/L_0 = 1.75$, an undulated parallel lamella structure and a hybrid structure consisting of both perpendicular and parallel lamellae occur. Although those degenerated structures are robust, they should be regarded as intermediate structures between the perpendicular lamellae and the parallel lamellae. Perpendicular lamellae reoccur at $D/L_0 = 1.83$, and furthermore the perpendicular lamella is the only observed structure at $D/L_0 = 1.83-2.0$. It is interesting to notice that for the gyroid-forming system with $f_A = 1/3$ its phase behavior under cylindrical confinement is dominated by lamellae when the pore is large ($D/L_0 > 1$), indicating that the system is more close to a lamella-forming one. However, there are differences in phase behavior between the gyroid-forming system and the lamella-forming one. One difference is that parallel lamellae have never been observed in the lamella-forming system when confined in a neutral pore, though they were observed for weakly preferential pores.[20,25] Another difference is that the thickness of each A-rich layer is much thinner than that of the B-rich layer in the gyroid-forming system, whereas these thicknesses are almost the same in the lamella-forming DBCPs.

Case 2: Majority-Selective Pores ($\alpha = 1$). In this case, the wall of the confining pore is strongly attractive to the majority blocks (B blocks) of the DBCPs. Typical morphologies obtained for DBCPs with $f_A = 0.3$ and $f_A = 1/3$ confined in cylindrical pores with $\alpha = 1$ are plotted in parts (a) and (b) of Figure 3, respectively. As shown in Figure 3a for $f_A = 0.3$, a series of complex structures are observed. When the pore is small ($D/L_0 \leq 0.17$), a chain of spheres appears at the center of the pore. The chain of spheres evolves into a straight cylinder at $D/L_0 = 0.25$. The diameter of the cylinder enlarges with increasing size of the pore, and a twisted band occurs at $D/L_0 = 0.75$. When D/L_0 is increased to 0.83, a novel catenarian structure, consisting of connected toroids, is observed, where the neighboring toroids are mutually perpendicular in orientations. This structure is different from the catenarian structures obtained for symmetric DBCPs when confined in cylindrical pore with weakly preferential surface.[19,25] For pores spanning a wide range of D/L_0 ($= 0.92-2.0$), one-ring perforated lamella parallel to the pore surface and related structures are observed. In order to clearly show these perforated lamella and the catenarian structures, their side views at different orientations are given in Figure S1. As shown in Figure 3a and Figure S1, one-ring perforated lamella with holes distributed in a low-symmetry fashion is observed at $D/L_0 = 0.92-1.08$, $1.4-1.5$, 1.67, and some large values due to the incommensurate pore size. For nearly commensurate pores with $D/L_0 = 1.17-1.33$, the holes within the perforated lamella are approximately hexagonally packed when the perforated lamella is stretched flat. The two degenerated structures

formed at $D/L_0 = 1.25-1.33$ are quite similar to each other but with different distances between neighboring holes. As shown in Figure S1, for the one-ring perforated lamella observed at $D/L_0 = 1.58$, the holes are also approximately hexagonally packed. One can conclude that the pore diameter strongly affects the distribution of the holes on the perforated lamella. The straight cylinder at the center of the pore is strongly elongated and evolves into a straight parallel lamella at $D/L_0 = 1.67-1.83$, and the latter evolves into stacked perpendicular cylinders at a large pore of $D/L_0 = 1.92$. For the structures of one-ring perforated lamella formed at $D/L_0 = 1.67-1.92$, it is interesting to notice that the holes are lined up along the same direction as that of the lamella or cylinder orientation, whereas there are no holes in the perpendicular direction. When $D/L_0 = 2.0$, two columns of stacked perpendicular short cylinders are formed inside the outer one-ring perforated lamella.

As shown in Figure 3b for the system with $f_A = 1/3$, a morphological sequence from a string of spheres to a cylinder to a straight band is again observed at small pores ($D/L_0 < 0.75$). The morphological sequence is similar to that observed in system with $f_A = 0.3$, except that a straight band is formed in this case, whereas a twist band is formed when $f_A = 0.3$. On the other hand, for large pores, the morphologies are quite different from those observed when $f_A = 0.3$. At $D/L_0 = 0.75$, a string of B-spheres occurs at the center of the band, and the structure is denoted as a 'spheres-embedded' band. A series of one-ring perfect lamella are observed in the range of $D/L_0 = 0.83-1.17$. The one-ring lamella is similar to that observed for symmetric DBCPs when confined in selective pores.[16−25] One-ring lamellar morphology was also observed for bulk cylinder-forming DBCPs confined in selective pores in a relatively weak segregation region.[28] At $D/L_0 = 1.25$, one-ring perforated lamella with a few randomly distributed holes occurs, since there are not sufficient A-blocks to form perfect lamella. With the increase of D/L_0 from 1.33 to 2.5, an outer one-ring perforated lamella remains, but the inner morphology varies from a straight cylinder to a straight band to two parallel cylinders to V-shaped perforated lamellae or two connected parallel lamellae to U-shaped perforated lamellae or two parallel lamellae to one-ring perforated lamella and a center straight cylinder to ε-shaped perforated lamellae to three parallel lamellae. The structures observed at $D/L_0 \approx 2.0$, the V-shaped perforated lamellae and the two parallel lamellae, are similar to the two-dimensional structure (denoted as LC_3 and LC_{LL}) obtained by Li et al. in their study of DBCPs with a volume fraction of $f_A \approx 0.36$ under circular confinement in a pore with a diameter of $17R_g$ using SCFT calculation.[18]

The morphologies shown in Figure 3 can be compared with those obtained from the cylinder- or lamella-forming DBCPs under the cylindrical confinement.[16−28] We notice that helices and stacked toroids, frequently observed in the cylinder-forming system inside majority-selective pores, never occur in the gyroid-forming systems. On the other hand, the concentric lamellae, frequently observed in the lamella-forming system, never occur for the gyroid-forming system with $f_A = 0.3$, and only the one-ring perfect lamella occurs in system with $f_A = 1/3$ at $D/L_0 = 0.83-1.17$. However, one-ring and two-ring concentric perforated lamellae are obtained for the gyroid-forming systems. The distribution of holes within the one-ring perforated lamella can be highly symmetric or asymmetric depending on the size of the pore. Inner parallel lamellae related structures, such as these observed at $D/L_0 = 2.0-2.5$ in Figure 3b, have not been observed before for bulk cylinder- or lamella-forming DBCPs when confined in strongly preferential pores.
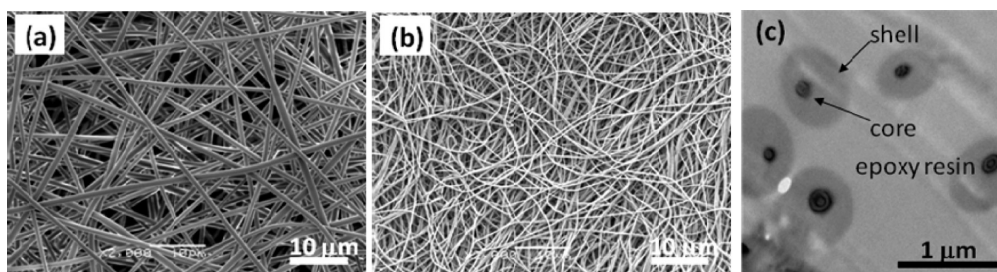
Figure 5. (a) SEM image of the PS-*b*-PDMS-75/PMAA core/shell fibers. (b) SEM image of the PS-*b*-PDMS-75 core fibers obtained from the removal of PMAA shell. (c) Cross-sectional TEM image of the core−shell fibers.

Case 3: Minority-Selective Pore ($\alpha = -1$). In this case, the minority A-blocks are attracted to the wall of the confining pore, forming a layer at the pore surface for large pores. Typical morphologies obtained for systems with $f_A = 0.3$ and $f_A = 1/3$ are plotted in parts (a) and (b) of Figure 4, respectively. For clarity, the outermost A-layer is not shown in the side views for large pores. As shown in Figure 4a for $f_A = 0.3$, the inner morphological sequence varies with increasing pore diameter from a string of spheres to a straight cylinder to a straight band to a helix to one-ring perforated lamella to a straight cylinder and an outer one-ring helix or stacked toroids to stacked perpendicular perforated lamellae. The holes within the (outer) one-ring perforated lamella are distributed in columns along the pore axis direction and are approximately hexagonally packed when the perforated lamella is stretched flat. The number of columns increases from two to three to four when the pore size is increased in the range of $D/L_0 = 1.42-1.67$. Just as in case 1 and case 2, the period of the S-helix and of the stacked toroids is $L_0/2$, while the distance between holes within the perforated lamella is smaller than L_0 but larger than $L_0/2$. One of the two degenerated structures at $D/L_0 = 1.83$ is a hybrid structure that consists of one layer of parallel lamella occupying half of the pore and stacked arcs perpendicular to the pore axis occupying the other half of the pore. At $D/L_0 = 2.0-2.08$, a new, stacked perpendicular perforated lamella structure occurs. The perpendicular perforated lamella structure is a compromise between stacked toroids and perpendicular lamellae, which may be due to the fact that the volume fraction of this gyroid-forming system is higher than that of the cylinder-forming one but lower than that of the lamella-forming one. Each layer in the stacked perpendicular perforated lamellae is in the shape of the figure θ. The inner morphological sequence shown in Figure 4a is quite different from that observed in case 2 (Figure 3a) and is also different from that obtained from cylinder-forming DBCPs located near the cylinder−sphere or cylinder−gyroid phase boundaries under the same confinement.[25−28] However, the inner morphologies of the structures with a straight cylinder and an outer one-ring helix or stacked toroids, shown in Figure 4a at $D/L_0 = 1.75-1.92$, are similar to the structures obtained when cylinder-forming DBCPs located near the cylinder-gyroid phase boundary are confined in majority block selective pores.[25]

For the morphologies shown in Figure 4b, a typical characteristic is that parallel lamellae or connected parallel lamellae are observed for large pores. At $D/L_0 = 1.83-1.92$, the inner structure, with two A-rich parallel lamellae, is very similar to the inner structure of the two-dimensional structure LC$_{LL}$ obtained by Li et al.[18] When D/L_0 is increased to 2.0 and 2.08, three connected A-rich parallel lamellae are observed. These inner structures are similar to the inner structures shown in Figure 3b at $D/L_0 = 2.5$.

At $D/L_0 = 1.5-1.67$, the one-ring perforated lamella or the outer one-ring perforated lamella and a central cylinder structures are observed, similar to the structures shown in Figure 4a at $D/L_0 = 0.9-1.5$. The morphologies shown in Figure 4a are similar to those shown in Figure 4b when the pore is small, whereas helices, stacked toroids, and perpendicular perforated lamellae observed in the former case are replaced with one-ring perforated lamellae or parallel lamellae in the latter case when the pore is large.

A common feature of Figures 2−4 is that morphologies exhibited by the two DBCPs with different f_A are similar to each other for small pores, but they are quite different for large pores. Comparing the morphologies shown in Figures 2−4 with those obtained from previous studies for systems with $f_A = 1/4$ or $1/6$, we notice that the inner morphological sequence for a system confined in pores that are selective for the minority block is more similar to that obtained for a system with a slightly lower volume fraction than the same system confined in pores that are selective for the majority block.[25,40] For example, some inner structures shown in Figure 4a are more similar to those for systems with $f_A = 1/4$ confined in majority-selective pores than those shown in Figure 3a,[25] and some inner structures shown in Figure 4b are more similar to those shown in Figure 3a than those in Figure 3b. Considering that a layer of minority blocks always forms at the pore surface for large minority-selective pores, this leads to a smaller effective volume fraction for the inner copolymers, so that the above observation seems reasonable. With a large enough pore diameter, this effect becomes inconspicuous, and the inner morphology for a system confined in minority block selective pores should be close to that obtained for the same system confined in majority block selective pores. This is the reason that when $D/L_0 \geq 2.0$, the inner structures shown in Figure 4b are similar to those shown in Figure 3b.

B. Experimental Morphologies of the Confined Systems. Parts (a) and (b) of Figure 5 show SEM images of the PS-*b*-PDMS-75/PMAA core/shell fibers and the PS-*b*-PDMS-75 core fibers after the removal of the PMAA shell using methanol as a selective solvent, respectively. The core/shell structures after annealing are shown by cross-sectional TEM images in Figure 5c. Figure 6 shows the microphase-separated morphologies of the block copolymer core in the annealed fibers. Concentric lamellar structures similar to those formed by lamella-forming DBCPs[7] are observed. This observation suggests that a fundamental phase transition, from gyroid to lamella, has occurred under the cylindrical confinement. This phase transition is probably induced by the preferred interfacial wetting at the core−shell interface. Compared with PDMS, PS has a lower Flory interaction parameter with PMAA ($\chi_{PS/PMAA} = 0.14$; $\chi_{PDMS/PMAA} = 0.72$ at 160 °C)[54] and therefore preferentially segregates to the core/shell interface with PMAA. This interfacial wetting of a PS layer on PMAA subsequently drives the formation of successive inner
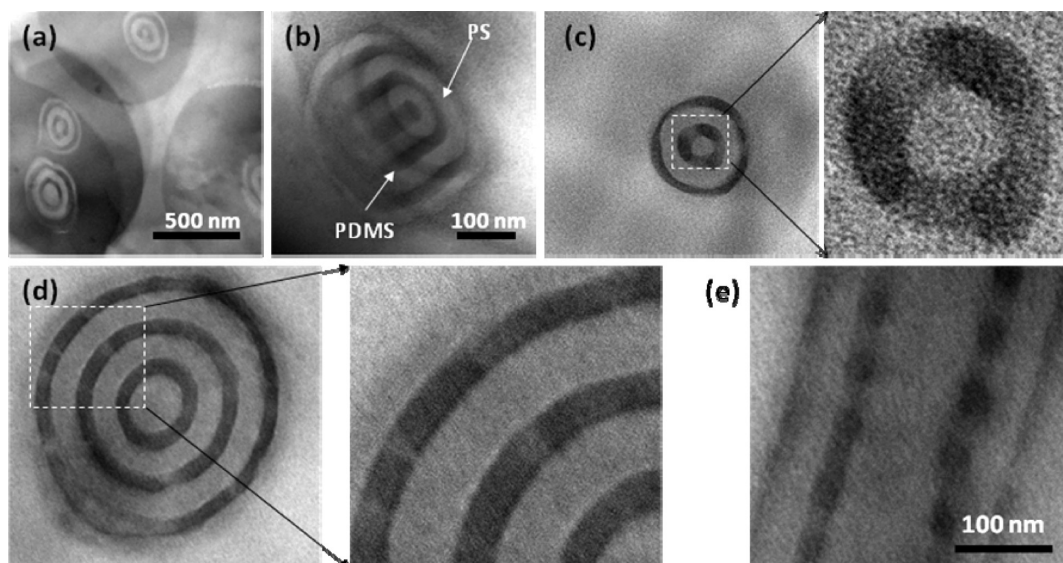
Figure 6. Cross-sectional TEM images of the PS-*b*-PDMS-75 DBCP under cylindrical confinement of different diameters. Note that the outermost PS monolayers are not well resolved in some cases due to the lack of contrast between PS and the PMAA shell. Images (b)−(d) have the same magnification.
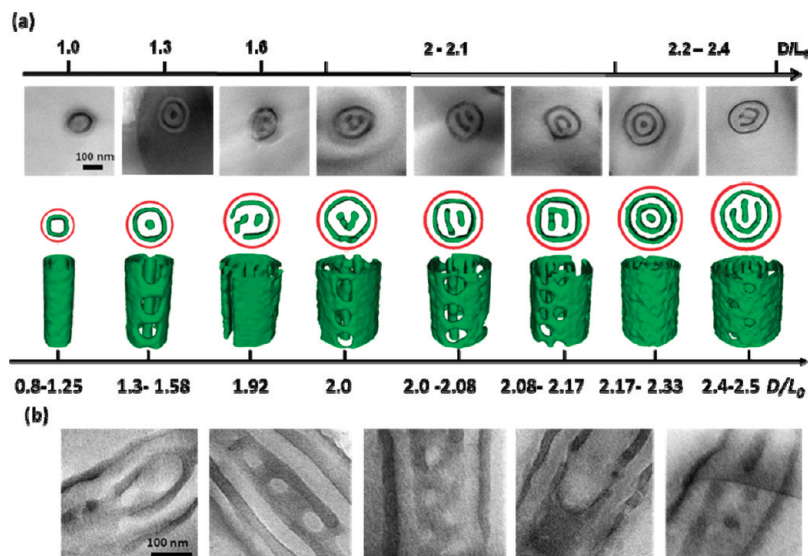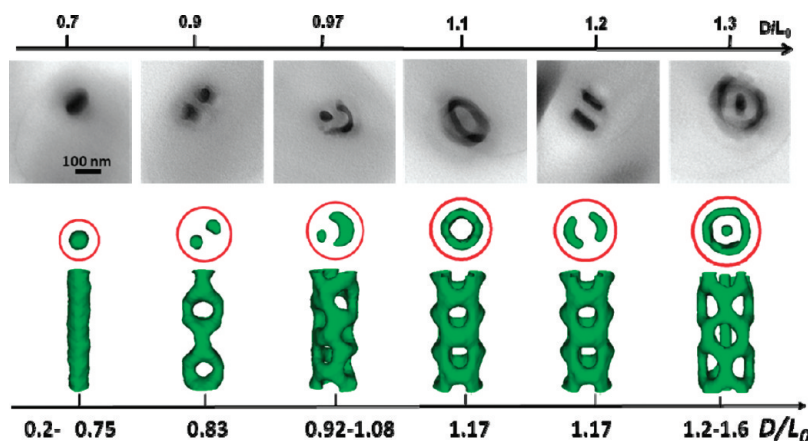

Figure 7. (a) Axial TEM images of the PS-*b*-PDMS-75 DBCP confined in electrospun fibers, showing variation in cross-sectional structure with fiber diameter. The normalized diameters (D/L_0) are labeled above the images. The values of D are obtained from TEM image analysis, while $L_0 = 6^{1/2} d_{211}$ is determined from SAXS. For comparison purposes, simulation results, both axial views and side views, are given. All experimental images have the same magnification. (b) Longitudinal TEM images of the PS-*b*-PDMS-75 DBCP confined in electrospun fibers. All images in (b) have the same magnification.

lamellar layers. A similar phase transformation was observed in thin (∼400 nm) films of the same polymer (PS-*b*-PDMS-75) confined between two flat PMAA layers.[55]

Similar to lamella-forming block copolymers,[30] the number of domains in the CL phase of cylindrically confined PS-*b*-PDMS-75 varies with the cores diameter, as shown by Figure 6. In some cases (e.g., Figure 6c−e) the PDMS domains show a periodic variation of contrast, suggesting that the PDMS lamella may be perforated in these cases. In bulk, the hexagonally perforated lamellar (HPL) phase appeared as metastable morphology intermediate between lamella and gyroids[5].

Besides the typical concentric lamellar morphology, other degenerated and novel morphologies were also observed for this PS-*b*-PDMS-75 copolymer annealed under identical thermodynamic conditions (i.e., 160 °C for 10 days under

vacuum). Figure 7a shows axial TEM cross sections of these unusual structures, along with the typical concentric lamellar morphology. In all these structures, the formation of an outermost PS layer (not resolved in some TEM images here) and the neighboring PDMS lamellar domain are probably due to the strong interfacial wetting between PS block and PMAA. However, for the domains further from the core/shell interface, intact lamellae are frequently surplanted by new structures that seem to be a combination of helical and perforated concentric lamellar motifs. The structures observed for PS-*b*-PDMS-75 include one-ring (perforated) lamella and outer one-ring (perforated) lamella with inner structure of one cylinder, two cylinders, V-shaped or U-shaped or ε-shaped (perforated) lamella, two parallel lamellae, and one cylinder and one-ring (perforated) lamella. Since PS is the majority component in this copolymer, our

Figure 8. Cross-sectional TEM images of the PS-*b*-PDMS-136 DBCP under cylindrical confinement, showing the novel morphologies. The normalized diameters are labeled above the images. For comparison purposes, simulation results, both axial views and side views, are given. All experimental images have the same magnification.

experimental conditions correspond to the case of the majority-selective pores (i.e., case 2 in the simulations). These structures are qualitatively consistent with the simulation results for model DBCPs with $f_A = 1/3$ confined in majority-selective pores. In order to rationalize the observed multiplicity of structures, a cross-sectional image from Figure 3b with $f_A = 1/3$ is reproduced below each of the TEM images. From this comparison, we see that the predicted results are qualitatively consistent with the experimental results over a relatively large range. Several longitudinal TEM images of the fibers are shown in Figure 7b. These may be compared with side views of the simulation images. At this stage, we have not observed experimentally all the structures predicted by simulations due to a number of technical limitations we have. The difficulty associated with sample preparation (e.g., cryo-microtoming), issues with TEM (e.g., beam damage), and the limitations on the range and variation of fiber core sizes only allow us to take a limited number of distinct observations. There are also kinetic issues of equilibrium and long-lived metastability in both experiments and simulations. Despite these limitations, the structures that are consistent with simulation ones are experimentally reproducible.[55]

Both the concentric lamellar structure and the novel structures were also observed for PS-*b*-PDMS-136 under cylindrical confinement. Figure 8 shows some representative TEM images of this polymer in annealed fibers. The novel structures observed here are similar to those formed by PS-*b*-PDMS-75. They include one or two (deformed) cylinders, one-ring (perforated) lamella, and one cylinder and outer one-ring (perforated) lamella. There structures are again qualitatively consistent with the simulation results for model DBCPs with $f_A = 0.3$ confined in majority-selective pores as compared in Figure 8.

Conclusion

The self-assembly of gyroid-forming DBCPs confined in cylindrical nanopores is investigated using a combination of simulations and experiments. With simulations, the effects of the pore size and surface selectivity on the equilibrium phase behavior are examined in detail. Two model DBCPs with volume fractions $f_A = 0.3$ and $f_A = 1/3$ are employed. It is predicted that pore selectivity, the size of the pore, and the volume fractions of DBCPs strongly influence the self-assembled morphology. In experiments, two DBCP samples, PS-*b*-PDMS-75 and PS-*b*-PDMS-136, with different molecular weights and slightly

different volume fractions are studied. Both form a gyroid phase in bulk. When these gyroid-forming DBCPs are encapsulated as the core component in the core/shell fibers fabricated by coaxial electrospinning, continuous fibers with a variety of microphase-separated morphologies are observed. Both simulations and experiments demonstrate that the gyroid-forming DBCPs under cylindrical confinement exhibit a very rich phase behavior. Some of these structures were very similar to those predicted or observed in the cylinder-forming or lamella-forming DBCPs under cylindrical confinement. This is probably due to the adjacency of gyroid phase to both the cylinder phase and lamella phase in the bulk phase diagram, and the confinement induces possible phase transitions. Other structures observed here seem to be unique for the compositions of the gyroid-forming block copolymers. It should be noted that some of the predicted morphologies could be a result of frustration between the constraints of radial confinement and the length scale of periodicity along the axis of the pore or fiber imposed during simulation; by relaxing this imposed axial length scale, a simpler morphological picture could ultimately emerge. Nevertheless, for a number of the morphologies predicted here, the results of both simulations and experiments are qualitatively in agreement.

Supporting Information Available: Figure S1 showing one-ring perforated lamella. This material is available free of charge via the Internet at http://pubs.acs.org.

References and Notes

(1) Fredrickson, G. H.; Bates, F. S. *Annu. Rev. Mater. Sci.* **1996**, *26*, 501.

(2) Park, C.; Yoon, J.; Thomas, E. L. *Polymer* **2003**, *44*, 6725.

(3) Hajduk, D. A.; Harper, P. E.; Gruner, S. M.; Honeker, C. C.; Kim, G.; Thomas, E. L.; Fetters, L. J. *Macromolecules* **1994**, *27*, 4063.

(4) Bates, F. S.; Schulz, M. F.; Khandpur, A. K.; Förster, S.; Rosedale, J. H.; Almdal, K.; Mortensen, K. *Faraday Discuss.* **1994**, *98*, 7.

(5) Hajduk, D. A.; Takenouchi, H.; Hillmyer, M. A.; Bates, F. S.; Vigild, M. E.; Almdal, K. *Macromolecules* **1997**, *30*, 3788.

(6) Tyler, C. A.; Morse, D. C. *Phys. Rev. Lett.* **2005**, *94*, 208302.

(7) Shin, K.; Xiang, H.; Moon, S. I.; Kim, T.; McCarthy, T. J.; Russell, T. P. *Science* **2004**, *306*, 76.

(8) Xiang, H.; Shin, K.; Kim, T.; Moon, S. I.; McCarthy, T. J.; Russell, T. P. *Macromolecules* **2004**, *37*, 5660.

(9) Xiang, H.; Shin, K.; Kim, T.; Moon, S. I.; McCarthy, T. J.; Russell, T. P. *J. Polym. Sci., Part B: Polym. Phys.* **2005**, *43*, 3377.

(10) Dobriyal, P.; Xiang, H.; Kazuyuki, M.; Chen, J.-T.; Jinnai, H.; Russell, T. P. *Macromolecules* **2009**, *42*, 9082.

(11) Xiang, H.; Shin, K.; Kim, T.; Moon, S. I.; McCarthy, T. J.; Russell, T. P. *Macromolecules* **2005**, *38*, 1055.

(12) Wang, Y.; Qin, Y.; Berger, A.; Yau, E.; He, C.; Zhang, L.; Gösele, U.; Knez, M.; Steinhart, M. *Adv. Mater.* **2009**, *21*, 2763.

(13) Sun, Y.; Steinhart, M.; Zschech, D.; Adhikari, R.; Michler, G. H.; Göele., U. *Macromol. Rapid Commun.* **2005**, *26*, 369.

(14) (a) Kalra, V.; et al. *Adv. Mater.* **2006**, *18*, 3299. (b) Kalra, V.; et al. *Small* **2009**, *5*, 2323. (c) Kalra, V.; et al. *Small* **2008**, *4*, 2067.

(15) Ma, M.; Krikorian, V.; Yu, J. H.; Thomas, E. L.; Rutledge, G. C. *Nano Lett.* **2006**, *6*, 2969.

(16) He, X.; Song, M.; Liang, H.; Pan, C. *J. Chem. Phys.* **2001**, *114*, 10510.

(17) Sevink, G. J. A.; Zvelindovsky, A. V.; Fraaije, J. G. E. M.; Huinink, H. P. *J. Chem. Phys.* **2001**, *115*, 8226.

(18) Li, W.; Wickham, R. A.; Garbary, R. A. *Macromolecules* **2006**, *39*, 806.

(19) Chen, P.; He, X.; Liang., H. *J. Chem. Phys.* **2006**, *124*, 104906.

(20) Feng., J.; Ruckenstein, E. *Macromolecules* **2006**, *39*, 4899.

(21) Wang, Q. *J. Chem. Phys.* **2006**, *126*, 024903.

(22) Sevink, G. J. A.; Zvelindovsky, A. V. *J. Chem. Phys.* **2008**, *128*, 084901.

(23) Feng., J.; Ruckenstein, E. *J. Chem. Phys.* **2006**, *125*, 164911.

(24) Feng, J.; Liu, H. L.; Hu, Y. *Macromol. Theory Simul.* **2006**, *15*, 674.

(25) Yu, B.; Sun, P.; Chen, T.; Jin, Q.; Ding, D.; Li, B.; Shi, A.-C. *J. Chem. Phys.* **2007**, *127*, 114906.

(26) Yu, B.; Sun, P.; Chen, T.; Jin, Q.; Ding, D.; Li, B.; Shi, A.-C. *Phys. Rev. Lett.* **2006**, *96*, 138306.

(27) Li, W.; Wickham, R. A. *Macromolecules* **2006**, *39*, 8492.

(28) Chen, P.; Liang, H.; Shi, A.-C. *Macromolecules* **2007**, *40*, 7329.

(29) Kleman, K. *Points, Lines, and Walls: In Liquid Crystals, Magnetic Systems and Various Ordered Media*; Wiley: Chichester, 1983.

(30) Ma, M.; Titievsky, K.; Thomas, E. L.; Rutledge, G. C. *Nano Lett.* **2009**, *9*, 1678.

(31) Thomas, E. L.; Anderson, D. M.; Henkee, C. S.; Hoffman, D. *Nature* **1988**, *334*, 598.

(32) (a) Kamperman, M.; Garcia, C. B. W.; Du, P.; Ow, H.; Wiesner, U. *J. Am. Chem. Soc.* **2004**, *126*, 14708. (b) Uehara, H.; Yoshida, T.; Kakiage, M.; Yamanobe, T.; Komoto, T.; Nomura, K.; Nakajima, K.; Matsuda, M. *Macromolecules* **2006**, *39*, 3971.

(33) Chan, V. Z.-H.; Hoffman, J.; Lee, V. Y.; Iatrou, H.; Avgeropoulos, A.; Hadjichristidis, N.; Miller, R. D.; Thomas, E. L. *Science* **1999**, *286*, 1716.

(34) (a) Kirkpatrick, S.; Gelatt, C. D.; Vecchi, M. P. *Science* **1983**, *220*, 671. (b) Kirkpatrick, S. *J. Stat. Phys.* **1984**, *34*, 975.

(35) Carmesin, I.; Kremer, K. *Macromolecules* **1988**, *21*, 2819.

(36) (a) Larson, R. G. *J. Chem. Phys.* **1992**, *96*, 7904. (b) Larson, R. G. *J. Chem. Phys.* **1989**, *91*, 2479.

(37) Chakrabarti, A.; Toral, R. *Phys. Rev. B* **1989**, *39*, 542.

(38) Grest, G. S.; Soukoulis, C. M.; Levin, K. *Phys. Rev. Lett.* **1986**, *56*, 1148.

(39) Yin, Y.; Sun, P.; Chen, T.; Li, B.; Jin, Q.; Ding, D.; Shi, A.-C. *ChemPhysChem* **2004**, *5*, 540.

(40) Yu, B.; Jin, Q.; Ding, D.; Li, B.; Shi, A.-C. *Macromolecules* **2008**, *41*, 4042.

(41) Yu, B.; Li, B.; Sun, P.; Chen, T.; Jin, Q.; Ding, D.; Shi, A.-C. *J. Chem. Phys.* **2005**, *123*, 234902.

(42) Metropolis, N.; Rosenbluth, A. W.; Rosenbluth, M. N.; Teller, A. H.; Teller, E. *J. Chem. Phys.* **1953**, *21*, 1087.

(43) Cochran, E. W.; Garcia-Cervera, C. J.; Fredrickson, G. H. *Macromolecules* **2006**, *39*, 2449.

(44) Cooke, D. M.; Shi, A.-C. *Macromolecules* **2006**, *39*, 6661.

(45) Wang, Q.; Nealey, P. F.; de Pablo, J. J. *Macromolecules* **2002**, *35*, 9563.

(46) Yin, Y.; Sun, P.; Jiang, R.; Li, B.; Chen, T.; Jin, Q.; Ding, D.; Shi, A.-C. *J. Chem. Phys.* **2006**, *124*, 184708.

(47) Fried, H.; Binder, K. *J. Chem. Phys.* **1991**, *94*, 8349.

(48) Hanley, K. J.; Lodge, T. P. *J. Polym. Sci., Part B: Polym. Phys* **1998**, *36*, 3101.

(49) Rutledge, G. C.; Fridrikh, S. V. *Adv. Drug Delivery Rev.* **2007**, *59*, 1384.

(50) Sun, Z.; Zussman, E.; Yarin, A. L.; Wendorff, J. H.; Greiner, A. *Adv. Mater.* **2003**, *15*, 1929.

(51) Yu, J. H.; Fridrikh, S. V.; Rutledge, G. C. *Adv. Mater.* **2004**, *16*, 1562.

(52) Li, D.; Xia, Y. *Nano Lett.* **2004**, *4*, 933.

(53) Politakos, N.; Ntoukas., E.; Avgeropoulos, A.; Krikorian, V.; Pate, B. D.; Thomas, E. L.; Hill, R. M. *J. Polym. Sci., Part B: Polym. Phys.* **2009**, *47*, 2419.

(54) *Polymer Handbook*, 4th ed.; Brandrup, J., Immergut, E. H., Grulke, E. A., Eds.; Wiley: New York, 1999; p VII/675.

(55) Ma, M. Ph.D Thesis, MIT, **2008**.